Geophysical Research Letters

RESEARCH LETTER
10.1029/2019GL084001

A New Perspective for Future Precipitation Change from Intense Extratropical Cyclones

C. Kodama[1], B. Stevens[2], T. Mauritsen[3], T. Seiki[1], and M. Satoh[4,1]

[1]Japan Agency for Marine-Earth Science and Technology, Yokohama, Japan, [2]Max Planck Institute for Meteorology, Hamburg, Germany, [3]Department of Meteorology, Stockholm University, Stockholm, Sweden, [4]Atmosphere and Ocean Research Institute, The University of Tokyo, Kashiwa, Japan

Key Points:
- The first global climate simulations to explicitly represent the mesoscale dynamics of extratropical cyclones are analyzed
- Precipitation from intense cyclones scales with temperatures across hemispheres and with global warming following Clausius-Clapeyron
- Projected change in precipitation from intense cyclones may thus be testable using global observations of precipitation in the present day

Supporting Information:
- Supporting Information S1

Correspondence to:
C. Kodama,
kodamac@jamstec.go.jp

Citation:
Kodama, C., Stevens, B., Mauritsen, T., Seiki, T., & Satoh, M. (2019). A New Perspective for Future Precipitation Change from Intense Extratropical Cyclones. *Geophysical Research Letters*, *46*, 12,435–12,444. https://doi.org/10.1029/2019GL084001

Received 6 JUN 2019
Accepted 18 SEP 2019
Published online 13 NOV 2019

Abstract Extratropical cyclones, major contributors to precipitation in the midlatitudes, comprise mesoscale fronts and fine-scale convective storms. Intense oceanic cyclones pose natural hazards, making reliable projections of their changes with global warming of great interest. Here, we analyze the first ever global climate simulations to resolve such mesoscale dynamics of extratropical cyclones. The present-day structure, frequency, and precipitation of the oceanic extratropical cyclones compare well with reanalyses and new satellite datasets that resolve the multiscale cloud-precipitation system. Simulated precipitation from intense oceanic cyclones increases at a rate of 7%/K^{1}, following Clausius-Clapeyron, with warming. The same scaling is apparent also in the interhemispheric contrast, suggesting that the latter could serve as a predictor of the former. Projected changes in precipitation from intense oceanic cyclones with warming may thus be testable using a reliable global observation network of precipitation in the present day.

Plain Language Summary Precipitation in midlatitudes is strongly governed by extratropical cyclones. Its future change is of great societal concern for adaptation to a warmer world. In this study, we use a new kind of global model and a new satellite dataset to resolve fine-scale and frontal features of cyclones and their changes with warming. The simulation shows that the amount of precipitation around the intense oceanic cyclones will increase due to global warming, and furthermore, the rate of precipitation change around the intense oceanic cyclones is closely related to the precipitation contrast between the northern and southern hemispheres in the present climate. This suggests that the future precipitation change associated with intense oceanic cyclones could be inferred from the difference between the northern and southern hemispheres in the present climate.

1. Introduction

The day-to-day weather in the midlatitudes is shaped by extratropical cyclones (ECs). Intense ECs are often associated with major weather hazards, including heavy precipitation and flash floods. Most of the precipitation in northern hemisphere (NH) storm-track regions (Hoskins & Valdes, 1990), as much as 80% in winter, can be attributed to ECs (Hawcroft et al., 2012). ECs are also associated with precipitation extremes, contributing more than half (regionally up to 80%) of extreme precipitation events (Pfahl & Wernli, 2012). In the Northeastern United States 93–100% of extreme precipitation in the winter comes from ECs (Agel et al., 2015). These are just some of the reasons why understanding how ECs, and the precipitation associated with them, will change with warming will be helpful for societies endeavoring to adapt to climate change (Bony et al., 2015).

The climatology of ECs, including precipitation and its response to climate change, has been studied using general circulation models (GCMs; Bengtsson et al., 2009; Champion et al., 2011; Field et al., 2008; Yettella & Kay, 2017; Zhang & Colle, 2017) as well as in regional models (Marciano et al., 2015; Michaelis et al., 2017; Willison et al., 2013). However, precipitation around ECs involves fine-scale dynamical and microphysical processes (Newton & Holopainen, 1991; Houze, 1993), and a horizontal resolution of hundreds to tens of kilometers, a typical resolution of GCMs, is thought to be inadequate for capturing intense area-averaged precipitation events (Bengtsson et al., 2009; Champion et al., 2011). Fine-mesh regional models can capture this structure, but only regionally, and require forcing from global models where many more aspects of the storms are parameterized. In addition, biases from these parameterizations may distort the coupling between heating and circulation in ECs simulated by GCMs (Willison et al., 2013). Past studies have also been hampered by the lack of a high-quality precipitation dataset that covers the storm-track regions with

a mesh size of less than 10 km (Field & Wood, 2007), particularly over the ocean and in the southern hemisphere (SH), where ground-based observation sites are sparse (Chen et al., 2008; Yatagai et al., 2009).

New satellite measurements are making it possible to investigate the fine-scale structure of ECs in both NH and SH. The Global Satellite Mapping of Precipitation (GSMaP; Kubota et al., 2007; Ushio et al., 2009)-Global Precipitation Measurement (GPM; Hou et al., 2014) product, a combined product of GPM microwave imager and existing multisatellite sensors, provides retrievals of precipitation distribution on the same scale as the simulations, and unlike Tropical Rainfall Measuring Mission (TRMM, Kummerow et al., 1998; Matsui et al., 2016; Roh & Satoh, 2014), GSMaP-GPM products extends well into the extratropics. In addition, the GPM dual-frequency precipitation radar (DPR) provides more accurate surface precipitation rate beneath the satellite orbit.

Climate change simulations were performed using a 14-km mesh global cloud-system resolving model, Nonhydrostatic Icosahedral Atmospheric Model (NICAM; Satoh et al., 2008, 2014; Tomita & Satoh, 2004), without parameterized convection (Kodama et al., 2015; Satoh et al., 2015). Such a fine global mesh makes it possible, for the first time, to use the underlying laws of fluid-dynamics, rather than parameterizations, to link the diabatic processes within ECs to the circulation systems they encompass, and to resolve the mesoscale features associated with their precipitation extremes in the context of global climate change. By resolving the fine-scale fluid motions and frontal dynamics of ECs, we address a chief limitation of earlier studies (Bengtsson et al., 2009; Champion et al., 2011). Ideally, a yet finer mesh model is required to resolve individual convective clouds (Kajikawa et al., 2016; Miyamoto et al., 2013); however, many of the statistical features of deep convection and their associated clouds are already reasonably represented in the 14-km mesh model (Noda et al., 2010, 2012; Kodama et al., 2012 and the references therein).

In this study, we use this new class of model, one more rooted in basic physics than those that have been used in the past (Satoh et al., 2019), and the observations that are also beginning to resolve the precipitation features of ECs. Conventionally, differences in dynamical characteristics as well as quality of observations often motivated people to analyze ECs in a particular hemisphere or region (e.g. Hoskins & Hodges, 2002; Hoskins & Hodges, 2005). Here, we test a new perspective that future changes in EC-precipitation might be identifiable in the difference of the present-day climate between the hemispheres, assuming dominant thermodynamic control over the dynamic one (Emori & Brown, 2005).

2. Methods

2.1. Simulation and Observational Datasets

We analyze output from an Atmospheric Model Intercomparison Project (AMIP)-type simulations by 14-km mesh NICAM of the present and a projected warmer climate. The simulations are fully described by Kodama et al. (2015) and Satoh et al. (2015), and some important aspects of the simulations are recapped here. The model is configured with 38 vertical levels up to a height of 40 km. The present-climate simulation (Kodama et al., 2015) was performed for June 1979–December 2008 following the AMIP protocol (Gates, 1992) except that a slab ocean model, with a depth of 15 m and nudged toward the observed historical sea surface temperature (SST) with a relaxation time of 7 days, was employed to better reproduce geographical distribution of precipitation. The future-climate simulation for June 2074–December 2099 follows the A1B scenario of Nakićenović and Swart (2000). For this future simulation, SST and sea ice concentrations were taken from the Coupled Model Intercomparison Project Phase 3 simulations following the methods described by Mizuta et al. (2008). The analysis of the output is restricted to hourly averaged precipitation and 6-hourly snapshots for mean sea-level pressure (MSLP), temperature, and winds. All fields are first interpolated to a longitude-latitude grid with a spatial resolution of 0.14°. The analysis periods of the present and future climate simulations are 1979–2003 and 2075–2099, respectively.

MSLP, temperature, and wind fields of the Japanese 55-year reanalysis (JRA-55) dataset (Harada et al., 2016; Kobayashi et al., 2015) were used to evaluate statistics and structures of ECs. Their temporal and spatial resolutions are 6 hourly and 1.25°. The GPM (Hou et al., 2014)-GSMaP (Kubota et al., 2007; Ushio et al., 2009) level 3 product (Version 04B), hourly 0.1°-gridded dataset extending from 60°S to 60°N, was used for evaluation of the simulated precipitation. In addition, precipitation derived from the GPM-DPR level 3 product (Version 04A, PrecipRateNearSurfMean), 0.25°-gridded orbital dataset, was temporally rearranged as 6-hourly dataset by collecting data over 3 hours before and after analysis time. Both liquid and solid

precipitations are considered in the GPM-GSMaP and GPM-DPR products. The analysis period of the observation and reanalysis is April 2014–March 2016.

2.2. Detection, Tracking, and Compositing Algorithms of the ECs

The EC detection and tracking algorithms are the same as those used in Kodama et al. (2014) except that the synoptic-filtered MSLP (Hoskins & Hodges, 2002) is used here for the EC detection. This change helps focus on synoptic-scale disturbances rather than background and smaller-scale fields such as polar lows. MSLP data are regridded to 2.5° in longitude and latitude before synoptic filtering to consistently detect EC centers using the model and reanalysis with different grid spacings (0.14° and 1.25°). Overall, the choice of detection and tracking algorithms does not influence the statistics of intense ECs, though it affects that of weaker ECs (Neu et al., 2013). Only the oceanic ECs that stay over the ocean for more than half of their lifetime are analyzed to reduce hemispheric asymmetry associated with moisture availability.

For compositing, a polar coordinate system centered on each EC is adopted to simplify spatial averaging and minimize grid distortion (Bengtsson et al., 2007). The composite of a field variable around the ECs is calculated by averaging it over all the scenes of ECs. Surface air temperature and precipitation amount are further averaged over all the points within 550 km (approximately 5° spherical cap; Bengtsson et al., 2009) from the center of the ECs. For the GPM-DPR, a weighting inversely proportional to the number of observations for each latitude is used for the above composite calculation to reduce a sampling bias associated with latitudinal non-uniformity of the observation. Because missing values exist for the precipitation amount derived from the GSMaP-GPM and GPM-DPR, surface air temperature at a grid point where precipitation amount is missing is masked for compositing and spatial averaging. Details of the above algorithms are described in supporting information S1.

3. Results

To help assess the fitness of the model to study how ECs change with warming, as we do in section 3.2, we first evaluate (in section 3.1) the simulations of present-day ECs, and the representation of EC structure, as compared to composites from satellite observations and reanalyses of meteorological data.

3.1. Simulated and Observed Oceanic ECs

In the reanalysis 9,121 and 16,226 oceanic ECs were identified in NH and SH, respectively. This compares favorably to the historical simulations over the same period for which 8,252 and 14,453 ECs were identified in the respective hemispheres. Dynamical features, like MSLP and low-level wind-speed, of the simulated ECs, Figures 1, 2a–2c, and S2, also compare well with that diagnosed from the reanalysis. Both the reanalysis and the simulation indicate that oceanic ECs generated in SH are more intense than those in NH, even if the simulated ECs are somewhat deeper than those identified in the reanalysis. This difference, also found in the result from ERA-Interim reanalysis (Dee et al., 2011; not shown), may be due to the coarse resolution of the reanalysis; as deeper, more intense ECs in the high-resolution model compared with coarser reanalysis were also reported by Bengtsson et al. (2009). Because of this different representation of the EC intensity between the reanalysis and the model, hereafter, the intense oceanic EC is defined as the most intense decile of oceanic ECs in terms of lifetime-minimum synoptic-filtered MSLP rather than adopting a fixed threshold of MSLP or windspeed.

Warming reduces the total number of oceanic ECs, but has no clearly discernible effect on EC intensity. For the conditions projected for 2075–2099, fewer (8,072 in NH and 14,060 in SH) oceanic ECs are simulated. Though the argument could be made, at least in SH, that there may be a slight increase in the number of intense ECs in the warmer climate (Figure 1, blue vs. red). And while such a change is consistent with a slight deepening in the composite mean synoptic-filtered MSLP (Figure 2c), to the extent such a signal is real, it is small. Further to this judgement, we also checked the closed contour size as a metric of EC size (Polly & Rossow, 2016) and find no clear changes with warming.

Taking the first 2 years of nearly-global GSMaP-GPM and orbital GPM-DPR data as a reference, we conclude that composite precipitation pattern of the ECs simulated by NICAM also compares well to what is observed, Figure 2. Peak precipitation is seen in the east and poleward side of the EC center, and the comma-like precipitation pattern characteristic of individual ECs is also evident in both the composite of intense oceanic ECs taken from the GSMaP-GPM data and the model output. A similar result (not shown) is found by

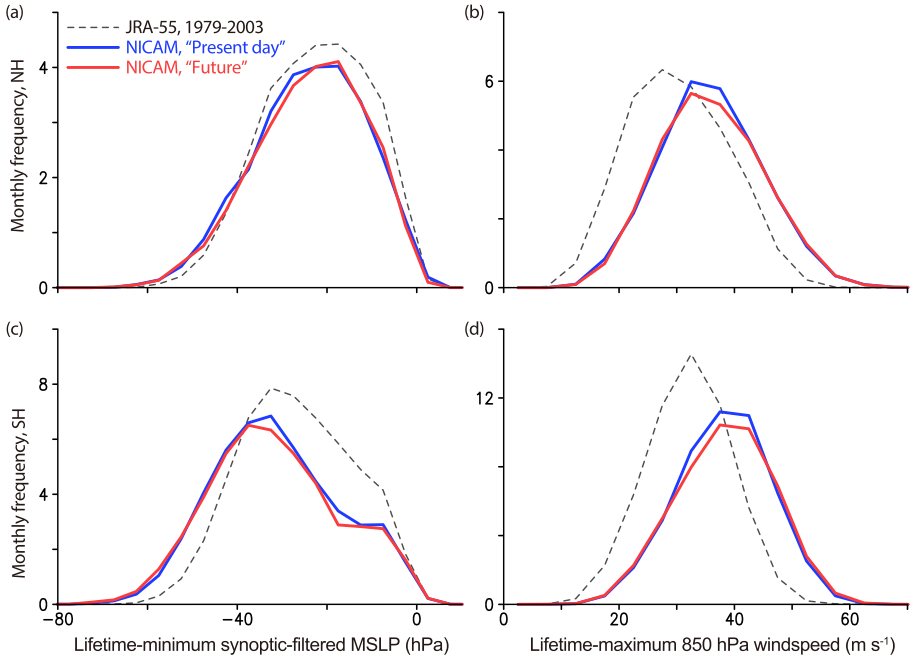

Figure 1. Monthly frequency of all the oceanic extratropical cyclones in northern hemisphere (NH; a and b) and southern hemisphere (SH; c and d) binned by lifetime-minimum synoptic-filtered mean sea level pressure (MSLP; left) and lifetime-maximum 850-hPa windspeed (right). Black, blue, and red lines show JRA-55 reanalysis over the period of 1979–2003, NICAM over 1979–2003, and NICAM over 2075–2099, respectively. Their bin sizes are 5 hPa and 5 m/s^{1}, respectively.

using the Integrated Multisatellite Retrievals for GPM grid product (IMERG) V05B (Huffman et al., 2018), which uses different retrieval algorithm. This type of qualitative similitude has also been documented in previous studies (Bauer & Del Genio, 2006; Field & Wood, 2007; Hawcroft et al., 2016). Albeit noisier, the GPM-DPR data shows quantitatively less peak precipitation, but the pattern is similar to that derived from the GSMaP-GPM data. Quantitative differences, to the extent they exist, appear to be dominated by the effects of limited observational coverage (supporting information Figure S3 and Text S2), rather than the small number of orbital samples for GPM-DPR, as discussed in Naud et al. (2018). We have also evaluated the precipitable water around the intense oceanic ECs and found the simulated storms to be very similar to that of JRA-55 reanalysis (not shown). Although these tests are not definitive, the available observations fail to identify substantial biases in the ability of the simulations to resolve the main structure of the precipitation system associated with intense oceanic ECs and thereby encourage our further analysis.

3.2. Relationship Between Inter-Hemispheric Contrast and Global-Warming Response in Precipitation From the Intense ECs

All of the observational data products consistently show that northern hemispheric ECs precipitate more on average than do their southern hemispheric counterparts, a tendency that is also captured by the simulations. Specifically, spatially-averaged precipitation amount over a 550-km radius circle about the center of intense oceanic ECs in NH versus SH is 10.7 mm/day^{1} versus 7.7 mm/day^{1} (GSMaP-GPM, 2 years), 7.4 mm/day^{1} versus 3.6 mm/day^{1} (GPM-DPR, 2 years), 9.4 mm/day^{1} versus 8.7 mm/day^{1} (IMERG, 2 years), and 8.8 mm/day^{1} versus 7.2 mm/day^{1} (NICAM, 25 years), showing a substantial variability among the different precipitation climatology partly due to the different data coverage. Such differences in intensity of precipitation in northern versus southern hemisphere intense oceanic ECs can be explained by differences in the surface air temperature and hence, the amount of moisture available to the storm. This is illustrated in Figure 3 (upper, blue triangles), which plots the simulated mean precipitation of the intense oceanic ECs versus the surface air temperature in the same region. The change in simulated precipitation with temperature is about $7\%/K^{1}$, which equals the expected rate of change in saturated vapor pressure by temperature, following the Clausius-Clapeyron equation.

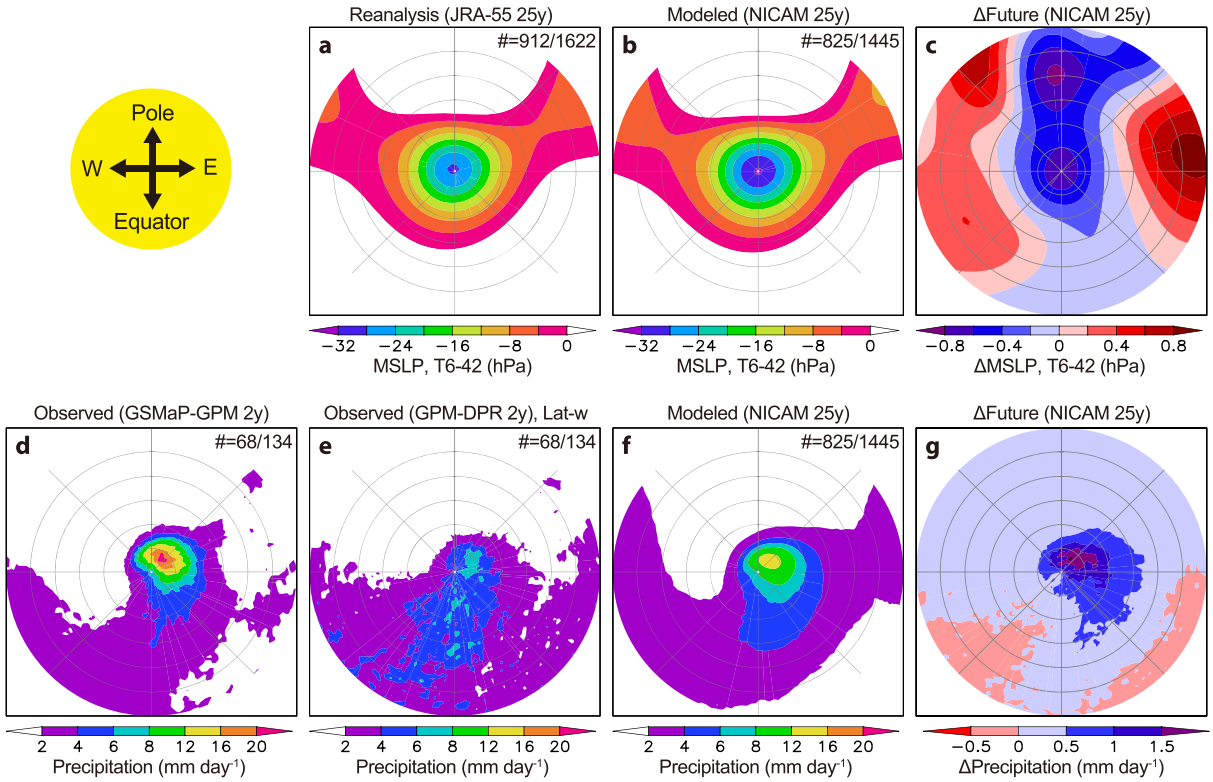

Figure 2. Composite of the synoptic-filtered MSLP (upper; Hectopascal pressure unit) and the precipitation amount (lower; millimeters per day) averaged over the intense oceanic ECs. (a) JRA-55 reanalysis for 1979–2003. (d) Global Satellite Mapping of Precipitation- Global Precipitation Measurement (GSMaP-GPM) for April/2014–March/2016. (e) GPM-dual-frequency precipitation radar (DPR) with latitudinal weighting (see section 2.2) for April/2014–March/2016. (b and f) Nonhydrostatic Icosahedral Atmospheric Model (NICAM) for 1979–2003. (c and g) Difference between NICAM for 1979–2003 and NICAM for 2075–2099. Gray circles show distances from the EC center by 500-km interval. The number of samples is shown as digit (NH/SH). Note that an observational coverage is 60°S–60°N for GSMaP-GPM and 65°S–65°N for GPM-DPR, respectively, and a dependency of the precipitation amount on the data coverage is shown in Figure S3 and Text S2.

If, as the simulation suggests, differences between precipitation in NH versus SH intense oceanic ECs can be explained by their temperature, rather than differences in their dynamic structure, changes in precipitation with warming within each hemisphere should scale likewise. This idea is supported by the simulations, as is illustrated in Figure 3 (upper, blue and red triangles), whereby the precipitation-temperature relationship of the NH and SH intense oceanic ECs with warming follows the same relationship that governs differences in NH versus SH intense oceanic ECs in the present day. The relationship is not sensitive to how intense oceanic ECs are identified, as it also holds when 850 hPa windspeed is used instead of MSLP (not shown). The relationship for the intense oceanic ECs also holds when averaging over a radius of 1,100 km (~10°) or 1,650 km (~15°) from EC center although for the 1,650-km radius, the rate of change in precipitation with temperature starts to become smaller (Figure S5). Similar scaling is found for all the oceanic ECs but with less rate of precipitation change by temperature (Figure 3, middle triangle).

The relatively small change in the dynamic structure of the ECs with warming that were discussed previously is consistent with a thermodynamic control on precipitation (see Text S2 for further analysis on dynamical response). A negligible dynamical response to global warming was also found in coarser resolution GCMs (Bengtsson et al., 2009), and the importance of the thermodynamics for the future change in EC-precipitation was already demonstrated using ensemble climate simulations (Yettella & Kay, 2017).

4. Discussion

A 7%/K^{1}, or Clausius-Clapeyron, scaling among the intense oceanic ECs in both different climates and the two hemispheres express a nontrivial symmetry of the Earth system. The scaling being independent of hemisphere is also evident, as would be expected for a thermodynamic argument, in moisture amounts (Figure S4) despite hemispheric asymmetries in the large-scale environment, for instance due to differences in

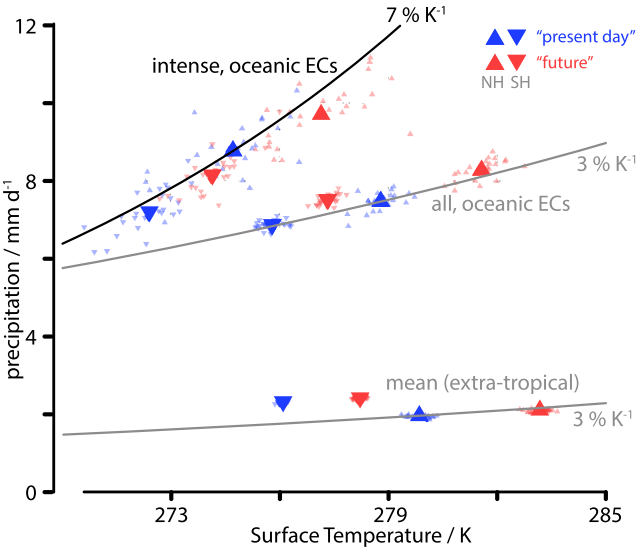

Figure 3. Surface air temperature and precipitation amount averaged over 550 km circle from the center of the intense oceanic extratropical cyclones (ECs; upper triangles) and all the oceanic ECs (middle triangles) and over the whole extratropics (lower triangles). Large (small) triangles show 25-year (annual) means for NH (▲) and SH (▼) from NICAM present (red) and future (blue) climate simulations. Black and gray lines show 7%/K^1 and 3%/K^1 curves passing at NH values of the 25-year NICAM present climate simulation.

land-sea contrast, orography, baroclinic zone, and direction of movement that might modify the scaling. Earlier studies pointed out an importance of the moisture convergence in precipitation increase due to SST rise (Field & Wood, 2007; Trenberth, 1999). A comparison of the oceanic and all the ECs shows that the interhemispheric relationship no longer holds when including land-based ECs (not shown), suggesting the importance of moisture availability around the ECs in the precipitation-temperature scaling. As we have seen in Figures 1 and 2, dynamical change in ECs due to global warming is negligible on a hemispheric scale. On a regional scale, dynamical changes could be more significant, as suggested or implied in past studies (Marciano et al., 2015; Michaelis et al., 2017; Pfahl & Sprenger, 2016; Zhang & Colle, 2017).

The change in precipitation for intense ECs is more than twice as large as what is expected (about 3%/K^1) based on energetic constraints on the mean precipitation (Allen & Ingram, 2002; Fläschner et al., 2016). Previous studies have hypothesized that it may, despite the energetic constraints, still increase following Clausius-Clapeyron scaling, or even more (Allen & Ingram, 2002; Paul R Field & Wood, 2007; Pall et al., 2007; Trenberth et al., 2003), particularly for intense ECs (Zhang & Colle, 2017). The present simulations suggest that the stronger increase is not a characteristic of the average ECs, but rather of the intense ECs. This might be due to a different precipitation-temperature scaling between convective and stratiform precipitation (Berg & Haerter, 2013; Berg et al., 2013), and in future studies, results from HighResMIP (Haarsma et al., 2016) will offer a chance to test to what extent these results can be reproduced by models running at coarser resolution with parameterized convection.

Based on these findings from the simulations, we hypothesize that precipitation from the intense oceanic ECs scale with temperature in a warmer climate in the same way that they scale with temperature in the present climate. An advantage of such a hemispheric breakdown over the global-mean perspective is the use of the temperature difference between hemispheres to efficiently constrain future precipitation change by increasing the number of samples (Figure 4a). A random sampling test using 2-,

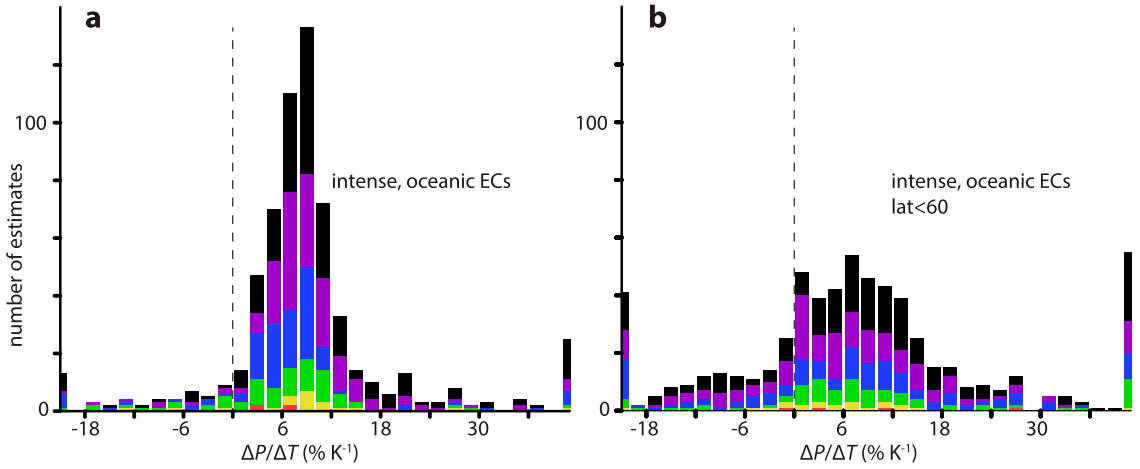

Figure 4. Histograms of the rate of change in precipitation by surface air temperature averaged over 550 km circle from the center of the intense oceanic extratropical cyclones (ECs) using a combination of annual NH and SH values. The rate of change can be estimated using NH values in particular year and SH values in particular year. Assume that the annual values are independent for each year and each hemisphere, we can obtain 625 estimations of the rate of change from the 25-year NICAM present climate simulation, as shown in all the colors in (a). Red, yellow, green, blue, and purple colors show results of a sensitivity test, in which 2-, 5-, 10-, 15-, 20-year data are sampled randomly to construct histograms as shown in red, yellow, green, blue, and purple colors. Results of another sensitivity test, in which the data are restricted to 60°S–60°N, is shown in (b).

5-, 10-, 15-, and 20-year NICAM data (Figure 4a, colors), which is repeated 1,000 times, shows about 90% of histograms have a peak between 4–12%/K^1 (roughly between half and double Clausius-Clapeyron scaling) using 5-year data and about 98 % using 10-year data. Hence, precipitation changes with temperature could be observable with as little as 5 years of data. We also tested for a sensitivity of the rate of precipitation change by temperature on data coverage. Figure 4b shows that the distribution in Figure 4a is broadened and skewed by restricting the model data to 60°S–60°N, the coverage of GSMaP-GPM product. Despite the limited record length and spatial coverage, the observed precipitation is highly correlated with temperature for each EC (Figure S4). However, the rate of change from observation is, until now, highly uncertain (29.5–39.0%/K^1 from GSMaP-GPM, 15.5–18.3%/K^1 from GPM-DPR, and 2.7–7.9%/K^1 from IMERG). We believe that such uncertainty reflects the preliminary state of the retrievals as well as the poor sampling statistics (Figure 4; see Text S3 and Figures S7 and S8 for further details). For instance, because the storm tracks are located in different latitudes in the two hemispheres, their statistics are differentially affected by the cut-off latitude and uncertainties in retrievals such as snowfall (Heymsfield et al., 2017; Kuo et al., 2016). Intense storms in the warmer NH often locate poleward of 60°N, which is the cut-off latitude of the GSMaP-GPM product. This sampling problem can thus be expected to worsen with future warming as the storm-tracks move poleward and hence, with time. If these shortcomings can be overcome in the data, our simulation and breakdown into the hemispheres suggest that the observations will provide critical tests of how precipitation from intense oceanic ECs will change with warming.

5. Concluding remarks

Simulations capable of resolving many of the fine-scale features of ECs over periods sufficiently long to assess the climatology of the most intense (upper decile of) ECs are analyzed. The simulation output compares favorably to newly available satellite measurements, which for the first time make it possible to infer precipitation on fine spatial and temporal scales. The simulations compare favorably to the satellite observations both in terms of the EC dynamical structure, quantitative precipitation amounts, and in terms of differences between ECs in the northern versus southern hemisphere.

The simulations further suggest that the dynamic structure of the intense ECs changes at most modestly in response to global warming and that surface air temperature, by setting the available moisture, determines the precipitation from intense oceanic ECs. Precipitation associated with intense oceanic ECs is found to depend on the surface air temperature following Clausius-Clapeyron scaling (7%/K^1), both when comparing hemispheric differences in the intense oceanic ECs and when comparing changes within a hemisphere in response to global warming. This suggests a degree of temperature-regulated precipitation invariance in intense oceanic ECs and is consistent with the finding that changes to the dynamic structure of the intense oceanic ECs with warming negligible. If, as our simulations suggest, precipitation around intense oceanic ECs increases with temperature following the scaling between intense oceanic ECs in the different hemispheres, then symmetries observed in the present climate may be informative of future changes.

Acknowledgments, Samples, and Data

The authors would like to thank two anonymous reviewers and editors for their patient and dedicated efforts. CK would like to thank Yohei Yamada, Masuo Nakano, and Tomoe Nasuno for technical support and/or discussion. GSMaP-GPM and GPM-DPR precipitation data are obtained from Japan Aerospace Exploration Agency (JAXA) G-Portal (https://gportal.jaxa.jp/gpr/?lang=en), JRA-55 reanalysis data from Japan Meteorological Agency (JMA; http://jra.kishou.go.jp/JRA-55/index_en.html), and IMERG precipitation data from National Aeronautics and Space Administration (NASA; https://pmm.nasa.gov/data-access/downloads/gpm). All the simulations were performed using the K computer at the RIKEN R-CCS (Proposal number hp120279, hp130010, and hp140219), and all the data to create Figure 1–4 are available on http://kodama.fubuki.info/wiki/wiki.cgi/research/paper_data. This study was supported by Integrated Research Program for Advancing Climate Models (TOUGOU), Program for Risk Information on Climate Change (SOSEI), and the FLAGSHIP2020 within the priority study4 (Advancement of meteorological and global environmental predictions utilizing observational "Big

Data"), which are promoted by the Ministry of Education, Culture, Sports, Science and Technology (MEXT), Japan. CK was supported by Taro Matsuno scholarship promoted by JAMSTEC and JSPS KAKENHI Grant JP17H04856. TM and BS received funding from the European Union H2020 programme under grant agreement no. 820829 during the final stages of this study. The authors declare no competing financial interests.

References

Agel, L., Barlow, M., Qian, J.-H., Colby, F., Douglas, E., & Eichler, T. (2015). Climatology of daily precipitation and extreme precipitation events in the Northeast United States. *Journal of Hydrometeorology*, *16*(6), 2537–2557. https://doi.org/10.1175/JHM-D-14-0147.1

Allen, M. R., & Ingram, W. J. (2002). Constraints on future changes in climate and the hydrologic cycle. *Nature*, *419*(6903), 224–232. https://doi.org/10.1038/nature01092

Bauer, M., & Del Genio, A. D. (2006). Composite analysis of winter cyclones in a GCM: Influence on climatological humidity. *Journal of Climate*, *19*(9), 1652–1672. https://doi.org/10.1175/JCLI3690.1

Bengtsson, L., Hodges, K. I., Esch, M., Keenlyside, N., Kornblueh, L., Luo, J.-J., & Yamagata, T. (2007). How may tropical cyclones change in a warmer climate? *Tellus A: Dynamic Meteorology and Oceanography*, *59*(4), 539–561. https://doi.org/10.1111/j.1600-0870.2007.00251.x

Bengtsson, L., Hodges, K. I. I., & Keenlyside, N. (2009). Will extratropical storms intensify in a warmer climate? *Journal of Climate*, *22*(9), 2276–2301. https://doi.org/10.1175/2008JCLI2678.1

Berg, P., & Haerter, J. O. (2013). Unexpected increase in precipitation intensity with temperature—A result of mixing of precipitation types? *Atmospheric Research*, *119*, 56–61. https://doi.org/10.1016/j.atmosres.2011.05.012

Berg, P., Moseley, C., & Haerter, J. O. (2013). Strong increase in convective precipitation in response to higher temperatures. *Nature Geoscience*, *6*(3), 181–185. https://doi.org/10.1038/ngeo1731 Bony, S., Stevens, B., Frierson, D. M. W., Jakob, C., Kageyama, M., Pincus, R. , et al. (2015). Clouds, circulation and climate sensitivity. *Nature Geoscience*, *8*(4), 261–268. https://doi.org/10.1038/ngeo2398

Champion, A. J., Hodges, K. I., Bengtsson, L. O., Keenlyside, N. S., & Esch, M. (2011). Impact of increasing resolution and a warmer climate on extreme weather from Northern Hemisphere extratropical cyclones. *Tellus A: Dynamic Meteorology and Oceanography*, *63*(5), 893–906. https://doi.org/10.1111/j.1600-0870.2011.00538.x

Chen, M., Shi, W., Xie, P., Silva, V. B. S., Kousky, V. E., Higgins, R. W., & Janowiak, J. E. (2008). Assessing objective techniques for gauge-based analyses of global daily precipitation. *Journal of Geophysical Research*, *113*, D04110. https://doi.org/10.1029/2007JD009132

Dee, D. P., Uppala, S. M., Simmons, A. J., Berrisford, P., Poli, P., Kobayashi, S., et al. (2011). The ERA-Interim reanalysis: Configuration and performance of the data assimilation system. *Quarterly Journal of the Royal Meteorological Society*, *137*(656), 553–597. https://doi.org/10.1002/qj.828

Emori, S., & Brown, S. J. (2005). Dynamic and thermodynamic changes in mean and extreme precipitation under changed climate. *Geophys. Res. Lett.*, *32*, L17706. https://doi.org/10.1029/2005GL023272

Field, P. R., Gettelman, A., Neale, R. B., Wood, R., Rasch, P. J., & Morrison, H. (2008). Midlatitude cyclone compositing to constrain climate model behavior using satellite observations. *Journal of Climate*, *21*(22), 5887–5903. https://doi.org/10.1175/2008JCLI2235.1

Field, P. R., & Wood, R. (2007). Precipitation and cloud structure in midlatitude cyclones. *Journal of Climate*, *20*(2), 233–254. https://doi.org/10.1175/JCLI3998.1

Fläschner, D., Mauritsen, T., & Stevens, B. (2016). Understanding the intermodel spread in global-mean hydrological sensitivity. *Journal of Climate*, *29*(2), 801–817. https://doi.org/10.1175/JCLI-D-15-0351.1

Gates, W. L. (1992). AMIP: The atmospheric model intercomparison project. *Bulletin of the American Meteorological Society*, *73*(12), 1962–1970. https://doi.org/10.1175/1520-0477(1992)073<1962:ATAMIP>2.0.co;2

Haarsma, R. J., Roberts, M. J., Vidale, P. L., Senior, C. A., Bellucci, A., Bao, Q., et al. (2016). High Resolution Model Intercomparison Project (HighResMIP v1.0) for CMIP6. *Geoscientific Model Development*, *9*(11), 4185–4208. https://doi.org/10.5194/gmd-9-4185-2016

Harada, Y., Kamahori, H., Kobayashi, C., Endo, H., Kobayashi, S., Ota, Y., et al. (2016). The JRA-55 reanalysis: Representation of atmospheric circulation and climate variability. *J. Meteor. Soc. Japan*, *94*(3), 269–302. https://doi.org/10.2151/jmsj.2016-015

Hawcroft, M., Dacre, H., Forbes, R., Hodges, K., Shaffrey, L., & Stein, T. (2016). Using satellite and reanalysis data to evaluate the representation of latent heating in extratropical cyclones in a climate model. *Climate Dyn.*. https://doi.org/10.1007/s00382-016-3204-6

Hawcroft, M. K., Shaffrey, L. C., Hodges, K. I., & Dacre, H. F. (2012). How much northern hemisphere precipitation is associated with extratropical cyclones? *Geophysical Research Letters*, *39*, L24809. https://doi.org/10.1029/2012GL053866

Heymsfield, A., Kramer, M., Wood, N. B., Gettelman, A., Field, P. R., & Liu, G. (2017). Dependence of the ice water content and snowfall rate on temperature, globally: Comparison of in situ observations, satellite active remote sensing retrievals, and global climate model simulations. *J. Appl. Meteor. Climatol.*, *56*(1), 189–215. https://doi.org/10.1175/JAMC-D-16-0230.1

Hoskins, B. J., & Hodges, K. I. (2005). A new perspective on southern hemisphere storm tracks. *Journal of Climate*, *18*(20), 4108–4129. https://doi.org/10.1175/JCLI3570.1

Hoskins, B. J., & Valdes, P. J. (1990). On the existence of storm-tracks. *J. Atmos. Sci.*, *47*(15), 1854–1864.

Hoskins, B. J., & Hodges, K. I. (2002). New perspectives on the northern hemisphere winter storm tracks. *Journal of the Atmospheric Sciences*, *59*(6), 1041–1061. https://doi.org/10.1175/1520-0469(2002)059<1041:NPOTNH>2.0.CO;2

Hou, A. Y., Kakar, R. K., Neeck, S., Azarbarzin, A. A., Kummerow, C. D., Kojima, M., et al. (2014). The global precipitation measurement mission. *Bull. Amer. Meteor. Soc.*, *95*(5), 701–722. https://doi.org/10.1175/BAMS-D-13-00164.1

Houze, R. Jr. (1993). *Cloud dynamics*, *International Geophysics* (Vol. *53*). Academic Press. https://www.elsevier.com/books/cloud-dynamics/houze-jr/978-0-12-356880-9

Huffman, G. J., Bolvin, D. T., Braithwaite, D., Hsu, K., Joyce, R., Kidd, C., et al. (2018). *NASA Global Precipitation Measurement (GPM) Integrated Multi-satellitE Retrievals for GPM (IMERG) Algorithm Theoretical Basis Document (ATBD) Version*, *5*, 2.

Kajikawa, Y., Miyamoto, Y., Yoshida, R., Yamaura, T., Yashiro, H., & Tomita, H. (2016). Resolution dependence of deep convections in a global simulation from over 10-kilometer to sub-kilometer grid spacing. *Progress in Earth and Planetary Science*, *3*(1), 1–14. https://doi.org/10.1186/s40645-016-0094-5

Kobayashi, S., Ota, Y., Harada, Y., Ebita, A., Moriya, M., Onoda, H., et al. (2015). The JRA-55 reanalysis: General specifications and basic characteristics. *Journal of the Meteorological Society of Japan. Ser. II*, *93*(1), 5–48. https://doi.org/10.2151/jmsj.2015-001

Kodama, C., Iga, S., & Satoh, M. (2014). Impact of the sea surface temperature rise on storm-track clouds in global nonhydrostatic aqua planet simulations. *Geophysical Research Letters*, *41*, 3545–3552. https://doi.org/10.1002/2014GL059972

Kodama, C., Noda, A. T. T., & Satoh, M. (2012). An assessment of the cloud signals simulated by NICAM using ISCCP, CALIPSO, and CloudSat satellite simulators. *Journal of Geophysical Research*, *117*. D12210. https://doi.org/10.1029/2011JD017317

Kodama, C., Yamada, Y., Noda, A. T., Kikuchi, K., Kajikawa, Y., Nasuno, T., et al. (2015). A 20-year climatology of a NICAM AMIP-type simulation. *Journal of the Meteorological Society of Japan. Ser. II*, *93*(4), 393–424. https://doi.org/10.2151/jmsj.2015-024

Kubota, T., Shige, S., Hashizume, H., Aonashi, K., Takahashi, N., Seto, S., et al. (2007). Global precipitation map using satellite-borne microwave radiometers by the GSMaP project: Production and validation. *IEEE Trans. Geosci. Remote Sens.*, *45*(7), 2259–2275. https://doi.org/10.1109/TGRS.2007.895337

Kummerow, C., Barnes, W., Kozu, T., Shiue, J., & Simpson, J. (1998). The tropical rainfall measuring mission (TRMM) sensor package. *Journal of Atmospheric and Oceanic Technology*, *15*(3), 809–817. https://doi.org/10.1175/1520-0426(1998)015<0809:TTRMMT>2.0.CO;2

Kuo, K.-S., Olson, W. S., Johnson, B. T., Grecu, M., Tian, L., Clune, T. L., et al. (2016). The microwave radiative properties of falling snow derived from nonspherical ice particle models. Part I: An extensive database of simulated pristine crystals and aggregate particles, and their scattering properties. *J. Appl. Meteor. Climatol.*, *55*(3), 691–708. https://doi.org/10.1175/JAMC-D-15-0130.1

Marciano, C. G., Lackmann, G. M., & Robinson, W. A. (2015). Changes in U.S. East Coast cyclone dynamics with climate change. *Journal of Climate*, *28*(2), 468–484. https://doi.org/10.1175/JCLI-D-14-00418.1

Matsui, T., Chern, J.-D., Tao, W.-K., Lang, S., Satoh, M., Hashino, T., & Kubota, T. (2016). On the land-ocean contrast of tropical convection and microphysics statistics derived from TRMM satellite signals and global storm-resolving models. *Journal of Hydrometeorology*, *17*(5), 1425–1445. https://doi.org/10.1175/JHM-D-15-0111.1

Michaelis, A. C., Willison, J., Lackmann, G. M., & Robinson, W. A. (2017). Changes in winter North Atlantic extratropical cyclones in high-resolution regional pseudo–global warming simulations. *Journal of Climate*, *30*(17), 6905–6925. https://doi.org/10.1175/JCLI-D-16-0697.1

Miyamoto, Y., Kajikawa, Y., Yoshida, R., Yamaura, T., Yashiro, H., & Tomita, H. (2013). Deep moist atmospheric convection in a subkilometer global simulation. *Geophysical Research Letters*, *40*, 4922–4926. https://doi.org/10.1002/grl.50944

Mizuta, R., Adachi, Y., Yukimoto, S., & Kusunoki, S. (2008). Estimation of the future distribution of sea surface temperature and sea ice using the CMIP3 multi-model ensemble mean CMIP3. *Technical Reports of the Meteorological Research Institute*, *56*, 1–28.

Nakićenović, N., & Swart, R. (Eds.). (2000). *IPCC special report on emissions scenarios*. Cambridge University Press.

Naud, C. M., Booth, J. F., Lebsock, M., & Grecu, M. (2018). Observational constraint for precipitation in extratropical cyclones: Sensitivity to data sources. *Journal of Applied Meteorology and Climatology*, *57*(4), 991–1009. https://doi.org/10.1175/JAMC-D-17-0289.1

Neu, U., Akperov, M. G., Bellenbaum, N., Benestad, R., Blender, R., Caballero, R., et al. (2013). IMILAST: A community effort to intercompare extratropical cyclone detection and tracking algorithms. *Bulletin of the American Meteorological Society*, *94*(4), 529–547. https://doi.org/10.1175/BAMS-D-11-00154.1

Newton, C. W., & Holopainen, E. O. (1991). *Extratropical cyclones. The Erik Palmén memorial volume*. (C W Newton & E. O. Holopanien, Eds.), *Quarterly Journal of the Royal Meteorological Society* (Vol. 117). American Meteorological Society. https://doi.org/10.1002/qj.49711750215

Noda, A. T., Oouchi, K., Satoh, M., & Tomita, H. (2012). Quantitative assessment of diurnal variation of tropical convection simulated by a global nonhydrostatic model without cumulus parameterization. *Journal of Climate*, *25*(14), 5119–5134. https://doi.org/10.1175/JCLI-D-11-00295.1

Noda, A. T., Oouchi, K., Satoh, M., Tomita, H., Iga, S., & Tsushima, Y. (2010). Importance of the subgrid-scale turbulent moist process: Cloud distribution in global cloud-resolving simulations. *Atmospheric Research*, *96*(2–3), 208–217. https://doi.org/10.1016/j.atmosres.2009.05.007

Pall, P., Allen, M. R., & Stone, D. A. (2007). Testing the Clausius-Clapeyron constraint on changes in extreme precipitation under CO2 warming. *Climate Dyn.*, *28*(4), 351–363. https://doi.org/10.1007/s00382-006-0180-2

Pfahl, S., & Sprenger, M. (2016). On the relationship between extratropical cyclone precipitation and intensity. *Geophysical Research Letters*, *43*, 1752–1758. https://doi.org/10.1002/2016GL068018

Pfahl, S., & Wernli, H. (2012). Quantifying the relevance of cyclones for precipitation extremes. *Journal of Climate*, *25*(19), 6770–6780. https://doi.org/10.1175/JCLI-D-11-00705.1

Polly, J. B., & Rossow, W. B. (2016). Cloud radiative effects and precipitation in extratropical cyclones. *Journal of Climate*, *29*(18), 6483–6507. https://doi.org/10.1175/JCLI-D-15-0857.1

Roh, W., & Satoh, M. (2014). Evaluation of precipitating hydrometeor parameterizations in a single-moment bulk microphysics scheme for deep convective systems over the tropical Central Pacific. *Journal of the Atmospheric Sciences*, *71*(7), 2654–2673. https://doi.org/10.1175/JAS-D-13-0252.1

Satoh, M., Matsuno, T., Tomita, H., Miura, H., Nasuno, T., & Iga, S. (2008). Nonhydrostatic icosahedral atmospheric model (NICAM) for global cloud resolving simulations. *Journal of Computational Physics*, *227*(7), 3486–3514. https://doi.org/10.1016/j.jcp.2007.02.006

Satoh, M., Tomita, H., Yashiro, H., Miura, H., Kodama, C., Seiki, T., et al. (2014). The Non-hydrostatic Icosahedral Atmospheric Model: Description and Development. *Progress in Earth and Planetary Science*, *1*(1), 18. https://doi.org/10.1186/s40645-014-0018-1 Satoh, M., Yamada, Y., Sugi, M., Kodama, C., & Noda, A. T. T. (2015). Constraint on future change in global frequency of tropical cyclones due to global warming. *J. Meteor. Soc. Japan*, *93*(4), 489–500. https://doi.org/10.2151/jmsj.2015-025

Satoh, M.,Stevens, B., Judt, F., Khairoutdinov, M., Lin, S.-J., Putman, W. M., & Düben, P. (2019). Global cloud-resolving models. *Current Climate Change Reports.* https://doi.org/10.1007/s40641-019-00131-0

Tomita, H., & Satoh, M. (2004). A new dynamical framework of nonhydrostatic global model using the icosahedral grid. *Fluid Dynamics Research*, *34*(6), 357–400. https://doi.org/10.1016/j.fluiddyn.2004.03.003

Satoh, M., Tomita, H., Yashiro, H., Miura, H., Kodama, C., Seiki, T., et al. (2014). The non-hydrostatic icosahedral atmospheric model: Description and development. *Progress in Earth and Planetary Science*, *1*(1), 18. https://doi.org/10.1186/s40645-014-0018-1

Trenberth, K. E. (1999). Conceptual framework for changes of extremes of the hydrological cycle with climate change. *Climatic Change*, *42*(1), 327–339. https://doi.org/10.1023/A:1005488920935

Trenberth, K. E., Dai, A., Rasmussen, R. M., & Parsons, D. B. (2003). The changing character of precipitation. *Bulletin of the American Meteorological Society*, *84*(9), 1205–1218. https://doi.org/10.1175/BAMS-84-9-1205

Ushio, T., Sasashige, K., Kubota, T., Shige, S., Okamoto, K., Aonashi, K., et al. (2009). A Kalman filter approach to the global satellite mapping of precipitation (GSMaP) from combined passive microwave and infrared radiometric data. *J. Meteor. Soc. Japan*, *87A*(SI), 137–151. https://doi.org/10.2151/jmsj.87A.137

Willison, J., Robinson, W. A., & Lackmann, G. M. (2013). The Importance of resolving mesoscale latent heating in the North Atlantic storm track. *Journal of the Atmospheric Sciences*, *70*(7), 2234–2250. https://doi.org/10.1175/JAS-D-12-0226.1

Kodama, C., Yamada, Y., Noda, A. T., Kikuchi, K., Kajikawa, Y., Nasuno, T., et al. (2015). A 20-year climatology of a NICAM AMIP-type simulation. *Journal of the Meteorological Society of Japan. Ser. II*, *93*(4), 393–424. https://doi.org/10.2151/jmsj.2015-024

Yatagai, A., Arakawa, O., Kamiguchi, K., & Kawamoto, H. (2009). A 44-Year daily gridded precipitation dataset for Asia based on a dense network of rain gauges. *SOLA*, *5*, 3–6. https://doi.org/10.2151/sola.2009

Yettella, V., & Kay, J. E. (2017). How will precipitation change in extratropical cyclones as the planet warms? Insights from a large initial condition climate model ensemble. *Climate Dynamics*, *49*(5–6), 1765–1781. https://doi.org/10.1007/s00382-016-3410-2

Zhang, Z., & Colle, B. A. (2017). Changes in extratropical cyclone precipitation and associated processes during the twenty-first century over Eastern North America and the Western Atlantic using a cyclone-relative approach. *Journal of Climate*, *30*(21), 8633–8656. https://doi.org/10.1175/JCLI-D-16-0906.1